JACS
JOURNAL OF THE AMERICAN CHEMICAL SOCIETY

ARTICLE

pubs.acs.org/JACS

Distribution of the Cationic State over the Chlorophyll Pair of the Photosystem II Reaction Center

Keisuke Saito,[†] Toyokazu Ishida,[‡] Miwa Sugiura,[§,∥] Keisuke Kawakami,[⊥] Yasufumi Umena,[#] Nobuo Kamiya,[⊥] Jian-Ren Shen,[▽] and Hiroshi Ishikita*[,†,∥]

[†]202 Building E, Career-Path Promotion Unit for Young Life Scientists, Graduate School of Medicine, Kyoto University, Yoshida-Konoe-cho, Sakyo-ku, Kyoto 606-8501, Japan

[‡]Nanosystem Research Institute (NRI), National Institute of Advanced Industrial Science and Technology (AIST), Tsukuba Central 2, 1-1-1 Umezono, Tsukuba, Ibaraki 305-8568, Japan

[§]Cell-Free Science and Technology Research Center, Ehime University, Bunkyo-cho, Matsuyama, Ehime, 790-8577, Japan

[∥]Precursory Research for Embryonic Science and Technology (PRESTO), Japan Science and Technology Agency (JST), 4-1-8 Honcho Kawaguchi, Saitama 332-0012, Japan

[⊥]Department of Chemistry, Graduate School of Science, and The OCU Advanced Research Institute for Natural Science and Technology (OCARINA), Osaka City University, Sumiyoshi, Osaka 558-8585, Japan

[#]Institute for Protein Research, Osaka University, 3-2 Yamadaoka, Suita, Osaka 565-0871, Japan

[▽]Division of Bioscience, Graduate School of Natural Science and Technology/Faculty of Science, Okayama University, Okayama 700-8530, Japan

Supporting Information

ABSTRACT: The reaction center chlorophylls *a* (Chl*a*) of photosystem II (PSII) are composed of six Chl*a* molecules including the special pair Chl*a* P_{D1}/P_{D2} harbored by the D1/D2 heterodimer. They serve as the ultimate electron abstractors for water oxidation in the oxygen-evolving Mn_4CaO_5 cluster. Using the PSII crystal structure analyzed at 1.9 Å resolution, the redox potentials of P_{D1}/P_{D2} for one-electron oxidation (E_m) were calculated by considering all PSII subunits and the protonation pattern of all titratable residues. The E_m(Chl*a*) values were calculated to be 1015−1132 mV for P_{D1} and 1141−1201 mV for P_{D2}, depending on the protonation state of the Mn_4CaO_5 cluster. The results showed that $E_m(P_{D1})$ was lower than $E_m(P_{D2})$, favoring localization of the charge of the cationic state more on P_{D1}. The $P_{D1}^{\bullet+}/P_{D2}^{\bullet+}$ charge ratio determined by the large-scale QM/MM calculations with the explicit PSII protein environment yielded a $P_{D1}^{\bullet+}/P_{D2}^{\bullet+}$ ratio of ∼80/∼20, which was found to be due to the asymmetry in electrostatic characters of several conserved D1/D2 residue pairs that cause the $E_m(P_{D1})/E_m(P_{D2})$ difference, e.g., D1-Asn181/D2-Arg180, D1-Asn298/D2-Arg294, D1-Asp61/D2-His61, D1-Glu189/D2-Phe188, and D1-Asp170/D2-Phe169. The larger $P_{D1}^{\bullet+}$ population than $P_{D2}^{\bullet+}$ appears to be an inevitable fate of the intact PSII that possesses water oxidation activity.

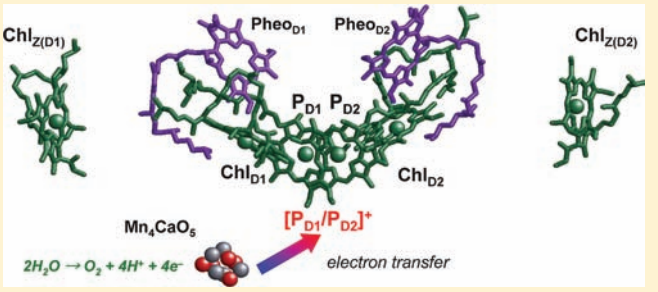

INTRODUCTION

The reaction center of photosystem II (PSII) is composed of the D1/D2 heterodimer, harboring the chlorophyll *a* (Chl*a*) pair P_{D1}/P_{D2}, the accessory Chl*a* Chl_{D1}/Chl_{D2}, two pheophytin *a* $Pheo_{D1}/Pheo_{D2}$, two quinones, and two additional Chl*a* $Chl_{Z(D1)}/Chl_{Z(D2)}$ as the redox active cofactors (Figure 1). P680, which absorbs light at a wavelength of 680 nm, is formed among these Chl*a* molecules. Excitation of P680 leads to the formation of the $Chl_{D1}^{\bullet+}$ $Pheo_{D1}^{\bullet-}$ state,[1−3] followed by the $[P_{D1}/P_{D2}]^{\bullet+}$ $Pheo_{D1}^{\bullet-}$ state. The resulting $[P_{D1}/P_{D2}]^{\bullet+}$ state serves as an electron abstractor for the oxygen-evolving cluster (OEC). Thus, water oxidation is ultimately achieved by the high redox potential for one-electron oxidation (E_m) of P680.

So far, the E_m(P680) value was not directly measured in experimental studies. On the other hand, the E_m(P680) value can be estimated mainly from measured E_m values of other cofactors. The E_m(P680) was first estimated to be 1.1 V by Klimov et al. in 1979 on the basis of the E_m(Pheo) value of −0.61 V measured at pH 11[4] and was soon supported by Rutherford et al., E_m(P680) = 1.1 V.[5] In contrast, very low values for E_m(P680), 0.8−0.9 V, were reported by Watanabe, Kobayashi, and co-workers.[6−8] After the PSII crystal structure from *Thermosynechococcus elongatus* was reported at 3.8 Å,[9] Rappaport et al. estimated

Received: April 29, 2011
Published: August 01, 2011

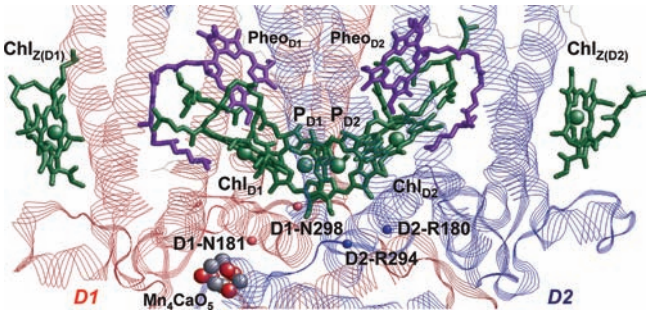

Figure 1. Chl*a* (green) in the D1/D2 heterodimer (red/blue) of PSII. Residues are represented by the backbone Cα atom potions.

E_m(P680) to be 1.26 V[10] on the basis of the measured $E_m(Q_A)$ value (= −30 mV by Rutherford, Krieger, and co-workers[11,12]) in PSII from *Synechocystis* PCC 6803 PSII,[10] which is higher than those reported before.[4,5] In 2005, Grabolle and Dau reported a similar value of 1.25 V.[13] On the basis of the PSII crystal structure at 3.0 Å resolution,[14] Ishikita et al. reported $E_m(P_{D1})$ and $E_m(P_{D2})$, i.e., E_m for monomer Chl*a*, to be 1.1−1.2 V by solving the linearized Poisson−Boltzmann equation and considering the protonation states of all titratable sites.[15] Recently, Kato et al. reported E_m(P680) = 1.17−1.21 V from the $E_m(Pheo_{D1})$ value of −0.5 V[16] measured at physiological pH (6.5) in PSII from *T. elongatus*. From these studies, it appears that E_m(P680) reaches 1.1−1.2 V (reviewed in refs 17−20), a value significantly higher than the E_m of monomeric Chl*a* in organic solvents.

Following the initial charge separation in the reaction center of PSII, the positive charge is distributed over P_{D1}/P_{D2}, resulting in a $P_{D1}^{\bullet+}/P_{D2}^{\bullet+}$ state. The $P_{D1}^{\bullet+}/P_{D2}^{\bullet+}$ ratio (or corresponding spin density distribution) was reported to be 82/18 from ENDOR studies of spinach PSII[21] or 80/20 from flash-induced spectroscopic studies of *Synechocystis* PCC 6803 PSII,[22] suggesting a preferential localization of the cationic state on P_{D1} over P_{D2} irrespective of the high similarity in the protein sequences between D1 and D2.[23] The reason for the asymmetric distribution of the cationic state is unknown due to the complexity of the PSII protein environment. Because of the difficulties in determining the individual $E_m(P_{D1})$ and $E_m(P_{D2})$ values experimentally owing to the strong coupling between these two Chl*a* molecules, it is essential to use reliable theoretical treatments to determine the individual $E_m(P_{D1})$ and $E_m(P_{D2})$ values, to elucidate the differences between these values, and to clarify the factors that contribute to these differences.

$E_m(P_{D1})$ and $E_m(P_{D2})$ have been calculated to be ∼1.2 V[15] based on the PSII structure reported at 3.2[14] and 2.9 Å[24] resolutions. Even in the first-principle approach, such as ab initio QM/MM calculations, the computational results largely depend on the reliability of the atomic coordinates of the protein structure. Although the previous PSII crystal structures contributed considerably to the elucidation of the detailed organization of polypeptide side chains and cofactors, the exact structure of the OEC moiety was not determined. There were also some uncertainties in the orientations of some amino acid side chains as well as some cofactors in the medium resolution structures, and no water molecules have been assigned in the crystal structure so far. Recently, the PSII crystal structure was reported at a resolution of 1.9 Å from *Thermosynechococcus vulcanus*, which revealed all of the components of the OEC cluster, giving rise to a chemical formula of Mn_4CaO_5.[25] In addition, all of the amino acid ligands for the OEC cluster were unambiguously assigned, and the structure and orientations of amino acid side chains and cofactors were determined at a much higher accuracy than those in the structures reported previously. This allows us to calculate $E_m(P_{D1})$ and $E_m(P_{D2})$ more accurately and to examine the influence of the OEC cluster and each of the amino acid side chains in the D1/D2 pair subunit on E_m(Chl*a*) precisely. Elucidating the difference between the $E_m(P_{D1})$ and $E_m(P_{D2})$ values and determining the factors that contribute to the difference may take us a step closer to answering the fundamental but not yet solved question of how the PSII protein environment modulates the Chl*a* cationic state distribution over the P_{D1}/P_{D2} pair.[21,22,26,27]

To answer the essential question of how the E_m level of each monomer Chl*a*—P_{D1} and P_{D2}—is situated in PSII, we calculated $E_m(P_{D1})$ and $E_m(P_{D2})$ values and attempted to clarify how the PSII protein environment modulates each E_m(Chl*a*), by using the 1.9 Å structure in the presence of the Mn_4CaO_5 cluster and by solving the linear Poisson−Boltzmann equation with consideration of the protonation states of all titratable sites in the entire PSII. By clarifying residues that influence $E_m(P_{D1})$ or $E_m(P_{D2})$, we will be able to pinpoint the protein components that are responsible for the measured ratio of ∼80/∼20 for the $P_{D1}^{\bullet+}/P_{D2}^{\bullet+}$ pair.[21,22]

Since the $E_m(P_{D1})$ and $E_m(P_{D2})$ values obtained represent those of monomeric Chl*a* and do not directly account for the $P_{D1}^{\bullet+}/P_{D2}^{\bullet+}$ ratio for the Chl*a* dimer, we also calculated the $P_{D1}^{\bullet+}/P_{D2}^{\bullet+}$ ratio for the P_{D1}/P_{D2} Chl*a* dimer using a large-scale quantum chemical/molecular mechanical (QM/MM) approach with the explicit treatment of the complete PSII atomic coordinates, defining the P_{D1}/P_{D2} dimer as the QM region and the remaining protein subunits-cofactors as the MM region. The full consideration of the OEC atoms, protein amino acid side chain characters, and backbone from all PSII protein subunits, and the bound water molecules, in the energetics of monomeric P_{D1} and P_{D2} as well as that of the P_{D1}/P_{D2} Chl*a* dimer pair will shed light on the mystery behind the energetic asymmetry of the D1/D2 electron transfer chains irrespective of the geometrical symmetry of the Chl*a* arrangement in the D1/D2 subunits.

■ COMPUTATIONAL PROCEDURES

In this article, we employed the following systematic modeling procedure: First, we constructed a realistic molecular model of the whole PSII complex using the recent high-resolution crystal structure. On the basis of this atomistic model, we evaluated the redox potential of P_{D1}/P_{D2} by solving the linear Poisson−Boltzmann equation with an explicit consideration of the protonation states for all titratable residues. Second, to obtain deeper insight into the electronic structure of the P_{D1}/P_{D2} Chl*a* dimer, which is the key molecule of the photosystem II reaction center, we performed large-scale QM/MM calculations for the entire PSII complex. Finally, after confirming the validity of the present computational results through the comparison with available experimental data, we searched for the atomistic origin that determines the asymmetric distribution of the cationic state of the P_{D1}/P_{D2} Chl*a* dimer. Technical details of each modeling procedure are summarized as follows.

Coordinates. The atomic coordinates of PSII were taken from the X-ray structure of the PSII complexes from *T. vulcanus* at 1.9 Å resolution (PDB code, 3ARC).[25] Hydrogen atoms were generated and energetically optimized with CHARMM,[28] whereas the positions of all non-hydrogen atoms were fixed and all titratable groups kept in their standard protonation states; i.e., acidic groups were ionized, and basic

groups were protonated. For the QM/MM calculations, we added additional counterions to neutralize the whole system.

Atomic Partial Charges. Atomic partial charges of the amino acids were adopted from the all-atom CHARMM22[29] parameter set. The charges of the protonated acidic O atoms were increased symmetrically by +0.5 unit charges to implicitly account for the presence of a proton. Similarly, instead of removing a proton in the deprotonated state, the charges of all of the protons of the basic groups of Arg and Lys were diminished symmetrically by a total unit charge. For residues for which the protonation states were not available in the CHARMM22 parameter set, appropriate charges were computed.[30] The atomic charges of the OEC cluster, Chl*a*, Pheo*a*, and quinones were determined by fitting the electrostatic potential in the neighborhood of these molecules by using the RESP procedure.[31] The electronic wave functions were calculated after geometry optimization with the DFT module in JAGUAR[32] (B3LYP/LACVP*) (Tables S1−4, Supporting Information).

OEC Models. In the S_1 state, the valences of the 4 Mn atoms are most probably (III, III, IV, and IV). The formal charges of the OEC components were assumed to be as follows: 2 Mn = +3, 2 Mn = +4, Ca^{2+} = +2, D1-Asp170, Glu189, Glu333, Asp342, Ala344, and CP43-Glu354 = −1 (deprotonated), D1-His332 = 0 (neutral), and CP43-Arg357 = +1 (protonated). The exact valences of the individual Mn atoms are unclear; however, we found that changing the charge distribution of each Mn atom from the above distribution did not affect our calculated results significantly (Table 1). The protonation states of the O atoms (and thus the net charge of the OEC atoms) in the OEC cluster remain unclear. Although O1, O2, and O3 are likely to be unprotonated O^{2-} based on observations of the OEC geometry, the protonation states of O4 linking Mn4 and Mn3 in the Mn_3CaO_4-cubane and O5 in one of the corners of the cubane linking Mn4 and the cubane necessitate more deep investigation as they might be O^{2-}, protonated OH^-, or even H_2O. Due to the uncertainty, we evaluated all possible combinations of the O4 and O5 protonation states (except the states where (O4, O5) are (H_2O, H_2O) and (O^{2-}, O^{2-})) and tentatively used the $O4H^-$ $O5H^-$ model (Table S1, Supporting Information). The OEC-depleted PSII was prepared by removing the Mn_4CaO_5 inorganic cluster and the two adjacent Cl^- ions, Cl^- 1 and Cl^- 2. Residues that were originally ligated to the Mn_4CaO_5 inorganic cluster were titrated. As a result, they were more protonated due to the absence of the positively charged Mn_4CaO_5 inorganic cluster.

Computation of E_m(Chl*a*). The present computation was based on the electrostatic continuum model, wherein we solved the linear Poisson−Boltzmann equation with the MEAD program.[33] To facilitate direct comparisons with previous computational results, identical computational conditions and parameters were used (e.g., refs 15 and 34) such as atomic partial charges and dielectric constants. The redox states of all other cofactors (e.g., Pheo*a* and quinones) were kept in their neutral charge states during the redox titration of each Chl*a*. The ensemble of the protonation patterns was sampled using the Monte Carlo method with the Karlsberg program[35] (Rabenstein, B. *Karlsberg online manual*, http://agknapp.chemie.fu-berlin.de/karlsberg/ (1999)). The dielectric constants were set to ε_p = 4 inside the protein and ε_w = 80 for water. All computations were performed at 300 K, pH 7.0, and an ionic strength of 100 mM. The linear Poisson−Boltzmann equation was solved using a three-step grid-focusing procedure at resolutions 2.5, 1.0, and 0.3 Å. The Monte Carlo sampling for a redox active group yielded the probabilities $[A_{ox}]$ and $[A_{red}]$ of the two redox states of the molecule A. E_m(Chl*a*) was evaluated using the Nernst equation. A bias potential was applied to obtain an equal amount of both redox states ($[A_{ox}] = [A_{red}]$), yielding the redox midpoint potential E_m as the resulting bias potential. For convenience, the computed E_m was given with millivolts accuracy without implying that the last digit is significant. In general, a few 10 mV in E_m is in a sufficiently reproducible range of our computational method.

Most recently, E_m(Chl*a*) values were reported to be +810 mV in acetonitrile and +860 mV in dimethylformamide.[36] Acetonitrile is known to ligate metals. A somewhat substantial background current in the anodic potential range is an inherent property of dimethylformamide, and the usage of other solvents was preferable for studies of Chl*a* oxidation.[6] On the other hand, the E_m(Chl*a*) value in CH_2Cl_2 was reported to be +800 mV (versus normal hydrogen electrode) with tetrabutylammonium perchlorate as the electrolyte.[37,38]

Chlorophylls possess high tendency to form self-aggregates in a various solvents, and this alters their electrochemical characteristic. The first oxidation potential of Chl*a*, E_m(Chl*a*), in CH_2Cl_2 was reported to be +800 mV vs NHE,[37] and the most recently reported E_m(Chl*a*) value in acetonitrile was +810 mV. Addition of a small amount of THF to CH_2Cl_2 or acetonitrile solution prevents the self-aggregation of bacteriochlorophyll *a* (BChl*a*), but the measured E_m(BChl*a*) for one-electron oxidation remains unchanged.[39] Addition of a small amount of THF to butyronitrile solution also prevents the self-aggregation of Chl*a*, and the E_m(Chl*a*) remains almost unchanged, +0.86 ∼ +0.87 V vs NHE.[40] Here, we used +800 mV vs NHE in CH_2Cl_2 because we previously considered the solvation energy difference between CH_2Cl_2 and water[15] and use the value of +698 mV as a reference E_m(Chl*a*) value in water in this work.

QM/MM Calculations. In all QM/MM calculations reported here, we employed the so-called electrostatic embedding QM/MM scheme and used the Qsite[41] program code. Electrostatic as well as steric effects created by complex PSII architecture were explicitly considered in all of the calculations. Due to the large system size of PSII, the QM region was limited to the P_{D1}/P_{D2} Chl*a* dimer for simplicity, while other protein units, all cofactors, and water molecules were approximated by the MM force field. Since we have optimized the atomic partial charges for the OEC cluster, Chl*a*, Pheo*a*, and quinones, the present QM/MM partition was accurate enough to describe the electronic structure of the $[P_{D1}/P_{D2}]^{\bullet+}$ Chl*a* dimer. To reliably determine the cationic character of the $[P_{D1}/P_{D2}]^{\bullet+}$ Chl*a* dimer, we employed the unrestricted DFT method with the B3LYP functional and LACVP* basis sets. The detailed geometry of the $[P_{D1}/P_{D2}]^{\bullet+}$ Chl*a* dimer was refined by the constrained QM/MM optimizations; the atomistic coordinates of the surrounding MM region were exactly fixed with the original X-ray coordinates. After obtaining the stable geometry of the QM fragment, we then determined the ESP charges for the cationic state of the $[P_{D1}/P_{D2}]^{\bullet+}$ Chl*a* dimer (Table S5, Supporting Information).

Possible Variations of the Calculated $E_m(P_{D1})$ and $E_m(P_{D2})$ Values. The calculated E_m values in the previous[15] and current computational studies are purely results of the interactions that solely originate from the original atomic coordinates of the PSII crystal structures[14,25] by assuming that the atomic coordinates or assignment of the protein side chain/cofactor chemical group orientations are appropriate. Since none of the atomic coordinates of the crystal structures are identical even in the same protein from the same species, it is reasonable that the calculated E_m values may differ in each crystal structure if the computational method is sufficiently precise.

Since the new structure had a remarkably higher resolution of 1.9 Å, it can be considered that the positions and orientations of side chains of amino acid residues, chemical groups of cofactors, and water molecules have been determined to a reasonably accuracy, and calculations based on this structure will provide more reliable values of E_m than those based on lower resolution structures. Although further improvement in the crystal resolution is possible, it is expected that not much new information or differences would be seen in a structure of PSII at an even higher resolution. Thus, calculation using a higher-resolution structure will basically yield the same results as obtained here. Nevertheless, possible variations of the calculated values using future PSII crystal structures may happen in the following cases: (i) the presence of another protein conformation near the focusing redox active site. For instance, there are two different conformations of the backbone atoms in the crystal structure of the G57T flavodoxin from *Clostridium beijerinckii* at 1.8 Å resolution.[42] The two protein conformations resulted in the two

Table 1. E_m(Chl*a*) Values for PSII Calculated for Different Protonation States of OEC (in mV)

net charge[a]	O4	O5	$E_m(P_{D1})$	$E_m(P_{D2})$
9	OH^-	H_2O	1138	1204
9	H_2O	OH^-	1126	1198
(average)			**1132**	**1201**
8	O^{2-}	H_2O	1089	1176
8	OH^-	OH^-	1065	1166
8	H_2O	O^{2-}	1054	1160
(average)			**1069**	**1167**
7	OH^-	O^{2-}	1001	1134
7	O^{2-}	OH^-	1028	1148
(average)			**1015**	**1141**
0 (OEC-depleted)	–[b]	–[b]	**953**	**1123**

[a] Net charge of the inorganic component Mn_4CaO_5 only, although we included the side chains of the OEC ligand residues in the DFT calculations of the atomic charges (Table S1, Supporting Information). [b] –, not applicable.

different calculated E_m/pK_a values of the flavin, only one of the two being in agreement with the experimentally measured value and accordingly the conformation being more relevant.[43] (ii) H-bond difference among the crystals. For bRC from *Rhodobacter sphaeroides*, there are several crystal structures available, exhibiting variations in H-bond geometry at the primary quinone Q_A for His-M219/Thr-M222 with N–O/O–O distances of 4.4/2.8 Å (2.8 Å resolution[44]), 3.2/3.6 Å (2.65 Å resolution[45]), or 2.8/3.6 Å (2.2 Å resolution[46]), which may be due to the absence of a strong H-bond, as suggested by FTIR studies.[47] Such variations of the H-bond pattern may also vary the calculated $E_m(Q_A)$ values in each crystal structure. This may, however, not hold true for P_{D1} and P_{D2} as their H-bond partners are not seen in the present crystal structure.[25]

RESULTS AND DISCUSSION

$E_m(P_{D1})$ and $E_m(P_{D2})$. The E_m(Chl*a*) values were calculated to be 1015–1132 mV for P_{D1} and 1141–1201 mV for P_{D2} (Table 1), depending on the protonation state of O4 and O5 atoms of the OEC cluster, based on the newly reported high-resolution structure of PSII.[25] These values are slightly lower than those calculated previously (1206 and 1222 mV for P_{D1} and P_{D2}, respectively[15]) based on the medium resolution PSII structure[14] partially due to the difference in the OEC cluster models. The $E_m(P_{D2})$ values were higher than the $E_m(P_{D1})$ values. These results indicate that the positively charged state of the P_{D1}/P_{D2} Chl*a* pair is localized more in P_{D1} than in P_{D2}; this is in agreement with the previous computational result,[15] but the difference between $E_m(P_{D1})$ and $E_m(P_{D2})$ was larger in the present study than that observed in the previous result irrespective of the protonation states of O4 and O5 (Table 1). The most significant difference between the present and the previous studies[15] is the OEC cluster model; OEC was composed of only four Mn and one Ca atoms, and no explicit O atoms were given in the previous crystal structure.[14] Thus, in the previous computational study, the influence of these atomic partial charges was implicitly considered in the constraining of the total charge of OEC: a charge of +2 was assigned to the Ca atom, and the remaining part of the total charge of the OEC cluster was divided by four and assigned to each Mn atom.[15] Thus, the calculated E_m values in the previous[15] and current computational studies are

Table 2. Influence of Protein Subunit Atomic Charges (Side Chain and Protein Backbone) on E_m(Chl*a*) (in mV)[a]

	$E_m(P_{D1})$	$E_m(P_{D2})$	ΔE_m
$Mn_4CaO_5 + 2Cl^-$	174	85	89
cofactors in D1/D2	6	23	–17
D1	–238	–65	–173
D2	67	92	–25
CP47	77	107	–30
CP43	43	22	21
PsbE	2	6	–4
PsbF	3	3	0
PsbH	–2	–3	1
PsbI	–1	0	–1
PsbJ	–14	–10	–4
PsbK	–4	–3	–1
PsbL	–31	–39	8
PsbM	3	5	–2
PsbO	42	44	–2
PsbT	–1	–2	1
PsbU	–24	–20	–4
PsbV	49	29	20
PsbX	1	2	–1
Ycf12 (Psb30)	1	1	0
PsbZ	0	–1	1
others	11	–30	41
total	164	246	–82

[a] ΔE_m represents $E_m(P_{D1}) - E_m(P_{D2})$.

results of the interactions that solely originate from the original atomic coordinates of the PSII crystal structures[14,25] by assuming that the atomic coordinates or assignment of the protein side chain/cofactor chemical group orientations are appropriate. For further discussions of possible alteration of the calculated E_m values, see Computational Procedures.

For the present Mn_4CaO_5 OEC cluster, an increase in the OEC net charge of 1 upshifts the $E_m(P_{D1})$ value by ~60 mV but only upshifts the $E_m(P_{D2})$ value by ~30 mV (Table 1) because the OEC cluster is located on the D1 side. The $E_m(P_{D1})$ and $E_m(P_{D2})$ values are not sensitive to the OEC protonation states unless the OEC net charge differs. In the OEC model where O4 and O5 are OH^- (the $O4H^-$ $O5H^-$ OEC model), the Mn_4CaO_5 region including Cl^- 1 and 2 is one of the major components that upshift E_m(Chl*a*) significantly (by 174 mV for P_{D1} and by 85 mV for P_{D2}, Table 2). Among the protein subunits, D2 and one of the antenna subunits CP47 significantly upshift $E_m(P_{D1})$ by ~70 mV and $E_m(P_{D2})$ by 90–110 mV (Table 2). In contrast, the D1 subunit dramatically downshifts $E_m(P_{D1})$ by 238 and $E_m(P_{D2})$ by 65 mV, demonstrating a striking difference from that of the D2 subunit, irrespective of the high similarity in their protein sequences.[23] It appears that, to energetically adjust the positively charged OEC cluster on the D1 side in PSII, there are more acidic and less basic residues on the D1 side than those on the D2 side.[15] In the following, we focus on the $O4H^-$ $O5H^-$ model unless otherwise specified.

Removal of the OEC Cluster. Although removal of the positively charged OEC cluster downshifted all E_m(Chl*a*) values, the E_m(Chl*a*) shifts were relatively small irrespective of the loss of the net charge of 7–9 (Table 1), implying alterations that had

Table 3. Ratios of Charge/Spin Distribution [%][a]

	charge		spin	
	$P_{D1}^{\bullet+}$	$P_{D2}^{\bullet+}$	P_{D1}	P_{D2}
complete PSII ($vinyl_{in}/vinyl_{out}$)	76.9	23.1	80.6	19.4
D1/D2 PSII ($vinyl_{in}/vinyl_{out}$)	71.6	28.4	75.7	24.3
(a) $\Delta[E_m(P_{D1})/E_m(P_{D2})$ difference increasing pairs] [b]	28.7	71.3	28.9	71.1
Δ(D1-Asn298/D2-Arg294)	61.7	38.3	65.7	34.3
Δ(D1-Asn181/D2-Arg180)	64.4	35.6	67.3	32.7
(b) $\Delta[E_m(P_{D1})/E_m(P_{D2})$ difference decreasing pairs] [c]	87.9	12.1	93.6	6.4
Δ(D1-Ala336/D2-Asp333)	75.1	24.9	80.1	19.9
Δ(D1-Met183/D2-Leu182)	74.7	25.3	79.1	20.9
P_{D1}-vinyl replaced by the P_{D2}-vinyl geometry [d] ($vinyl_{out}/vinyl_{out}$)	74.6	25.4	78.3	21.7
P_{D2}-vinyl replaced by the P_{D1}-vinyl geometry [d] ($vinyl_{in}/vinyl_{in}$)	70.0	30.0	76.0	24.0
P_{D1}/P_{D2}-vinyl swapped [d] ($vinyl_{out}/vinyl_{in}$)	72.9	27.1	78.6	21.4
P_{D1}-phytol replaced by the P_{D2}-phytol geometry [d]	65.5	34.5	69.7	30.3
phytol deleted P_{D1}/P_{D2} [d]	67.1	32.9	70.6	29.4

[a] Δ stands for deletion of atomic charges. For atomic partial charges of $[P_{D1}/P_{D2}]^{\bullet+}$ (unrestricted DFT/B3LYP functional, LACVP*), see Table S5, Supporting Information. [b] Residues listed in Table 4a. [c] Residues listed in Table 4b. [d] See Figure S1, Supporting Information, for the geometry.

occurred to partially compensate for the loss of the OEC cluster. The compensation effect is due to protonation at titratable residues in the D1 subunit, and these residues are mainly (i) the OEC ligand residues[25] D1-Asp170 (proton uptake by ~1.0 H^+), D1-Glu333 (~0.3 H^+), and D1-Asp342 (~0.9 H^+) and (ii) those proposed to participate in a possible proton exit pathway or the H-bond network linked with the OEC,[48−52] i.e., D1-Asp61 (~0.6 H^+) and D1-Glu65 by ~0.4 H^+. These residues were essentially ionized in the presence of the OEC cluster. The observed changes in the protonation states of the latter residues imply that D1-Asp61 and D1-Glu65 are under strong influence of the OEC cluster in the intact PSII.

Cationic State Is Localized More in P_{D1} than P_{D2}. The $E_m(P_{D1})$ and $E_m(P_{D2})$ values were calculated to be 1065 and 1166 mV, respectively, in the $O4H^-$ $O5H^-$ OEC model. The $E_m(P_{D2})$ value was higher than the $E_m(P_{D1})$ value; this is in agreement with the previous result.[15] These results indicate that the positively charged state of the P_{D1}/P_{D2} Chl*a* pair is localized more in P_{D1} than in P_{D2}.

The $P_{D1}^{\bullet+}/P_{D2}^{\bullet+}$ ratio was calculated to be 76.9/23.1 in the complete PSII based on the 1.9 Å resolution structure (Table 3). This ratio is lower than that expected from the difference in the E_m values between the two pigments, as a difference of 100 mV in the E_m values will result in a $P_{D1}^{\bullet+}/P_{D2}^{\bullet+}$ ratio of 98/2 if we use a simple consideration of the Boltzmann distribution. However, this situation does not apply to P_{D1}/P_{D2} since the two pigments are electronically coupled. In FTIR studies of *T. elongatus* PSII,[27,53] 70−80% of the cationic state was localized on one of the P_{D1}/P_{D2} Chl*a* units, although the assignment of the dominant species to P_{D1} or P_{D2} was not possible. Since the *T. elongatus* PSII[14,24] shares high structural similarities with the *T. vulcanus* PSII,[25] the $P_{D1}^{\bullet+}/P_{D2}^{\bullet+}$ ratio observed in the FTIR studies[27,53] can be assigned to be 70−80/30−20 based on the present study.

The spin density distribution calculated for the wild type was 80.6/19.4 (Table 3), which is close to the experimentally obtained values of 82/18 from ENDOR studies of spinach PSII[21] or 80/20 from flash-induced spectroscopic studies of *Synechocystis* PCC 6803 PSII.[22] Note that the calculated spin density distribution was more asymmetric than that of the charge distribution, a fact already pointed out previously.[53,54]

Influence of the Protein Subunits Other than D1/D2 on the $P_{D1}^{\bullet+}/P_{D2}^{\bullet+}$ Ratio. The P_{D1}/P_{D2} pair is embedded in the D1/D2 subunits, which are further surrounded by the antenna complexes CP43/CP47. The charge influence of the entire CP43/CP47 subunit pair on E_m(Chl*a*) was calculated to be 120 mV for $E_m(P_{D1})$ and 129 mV for $E_m(P_{D2})$ (Table 2), yielding no significant difference in the $E_m(P_{D1})/E_m(P_{D2})$ pair. The combination of all of the remaining PSII subunits except D1/D2 also resulted in no significant differences for the $E_m(P_{D1})/E_m(P_{D2})$ pair. By contrast, the entire D1/D2 subunit pair downshifted $E_m(P_{D1})$ by 171 mV but upshifted $E_m(P_{D2})$ by 27 mV, resulting in an E_m difference of 198 mV between P_{D1} and P_{D2}. Thus, a key to understanding the $E_m(P_{D1})/E_m(P_{D2})$ difference lies predominantly in the D1/D2 environment. Although the D1 and D2 proteins have high similarity in their protein sequences (Figure 2),[23] we found that there were a number of residue pairs that produced the $E_m(P_{D1})/E_m(P_{D2})$ difference (Table 4).

To investigate the influences of protein subunits and cofactors on the $P_{D1}^{\bullet+}/P_{D2}^{\bullet+}$ ratio, we removed all of the atomic coordinates except for the D1/D2 heterodimer proteins and the cofactors harbored by these two subunits (D1/D2-PSII). In this D1/D2-PSII, the $P_{D1}^{\bullet+}/P_{D2}^{\bullet+}$ ratio was calculated to be 71.6/28.4 (Table 3), which is not altered significantly compared to the complete PSII. Hence, the $P_{D1}^{\bullet+}/P_{D2}^{\bullet+}$ ratio of ~80/~20 in the entire PSII essentially originates from the D1/D2 heterodimer proteins and the cofactors associated with them. This coincided with the above results that the D1/D2 heterodimer proteins are the major regions that induce the $E_m(P_{D1})/E_m(P_{D2})$ difference due to the differences in the D1/D2 amino acid sequence (Table 2). Note that the heavy atom positions of the two subunits and cofactors in the D1/D2-PSII structure are the same as those in the complete PSII structure.

In contrast, FTIR studies of *T. elongatus* PSII by Okubo et al. indicated that the $P_{D1}^{\bullet+}/P_{D2}^{\bullet+}$ ratio was ~50/50 in the PSII that is comprised of only D1, D2, and cytochrome *b*559 subunits (D1/D2/cyt*b*559-PSII).[53] The discrepancy of the $P_{D1}^{\bullet+}/P_{D2}^{\bullet+}$ ratio from the present result of D1/D2-PSII (71.6/28.4) implies that the structure of the isolated D1/D2/cyt*b*559-PSII complex

```
     1          11         21         31         41         51
D1   MTTTLQRRES ANLWERFCNW VTSTDNRLYV GWFGVIMIPT LLAATICFVI AFIAAPPVDI
D2   MTIAIGRAPA ERGWFDILDD WLKRDRFVFV GWSGILLFPC AYLALGGWLT GTTFVTSWYT
     1          11         21         31         41         51

     61         71         81         91         101        108
D1   DGIREPVSGS LLYGNNIITG AVVPSSNAIG LHFYPIWEAA S---LDEWLY NGGPYQLIIF
D2   HGLAS----S YLEGCNFLTV AVSTPANSMG HSLLLLWGPE AQGDFTRWCQ LGGLWTFIAL
     61         67         77         87         97         107

     118        128        138        148        158        168
D1   HFLLGASCYM GRQWELSYRL GMRPWICVAY SAPLASAFAV FLIYPIGQGS FSDGMPLGIS
D2   HGAFGLIGFM LRQFEIARLV GVRPYNAIAF SAPIAVFVSV FLIYPLGQSS WFFAPSFGVA
     117        127        137        147        157        167

     178        188        198        208        218        228
D1   GTFNFMIVFQ AEHNILMHPF HQLGVAGVFG GALFCAMHGS LVTSSLIRET TETESANYGY
D2   AIFRFLLFFQ GFHNWTLNPF HMMGVAGVLG GALLCAIHGA TVENTLFQDG -EGASTFRAF
     177        187        197        207        217        -

     238        248        258        268        278        288
D1   KFGQEEETYN IVAAHGYFGR LIFQYASFNN SRSLHFFLAA WRVVGVWFAA LGISTMAFNL
D2   NPTQAEETYS MVTANRFWSQ IFG--IAFSN KRWLHFFMLF VPVTGLWMSA IGVVGLALNL
     236        246        256        264        274        284

     298        307        317        327        337
D1   NGFNFN-HSV IDAKGNVINT WADIINRANL GMEVMHERNA HNFPLDLA
D2   RSYDFISQEI RAAEDPEFET FYTKNLLLNE GIRAWMAPQD QPHENFVFPE EVLPRGNAL
     294        304        314        324        334        344
```

Figure 2. Amino acid sequence of the D1 and D2 subunits from *T. vulcanus*. D1/D2 residue pairs in each line were generated from the protein sequence alignment performed with the CLUSTAL program[67].

may be significantly different from the intact PSII structure. Indeed, Okubo et al. concluded that the structure and the electronic properties of P680 were considerably modified in the isolated D1/D2/cyt*b*559-PSII,[53] which could explain the discrepancy from the $P_{D1}^{\bullet+}/P_{D2}^{\bullet+}$ ratio of D1/D2-PSII calculated in the present study. Hence, the actual removal of the protein subunits that surround the D1/D2 heterodimer may also induce conformational changes in the D1/D2 protein.[55]

D1/D2 Residue Pairs That Contribute to the Larger $P_{D1}^{\bullet+}$ Population. *(a) $E_m(P_{D1})/E_m(P_{D2})$ Difference.* Among the D1/D2 residue pairs, six residue pairs contributed to increase the $E_m(P_{D1})/E_m(P_{D2})$ difference by more than 20 mV (Table 4a), whereas five residue pairs contributed to decrease the difference by more than 20 mV (Table 4b). Furthermore, the decrease in the $E_m(P_{D1})/E_m(P_{D2})$ difference due to the five residue pairs was obviously smaller than the increase in the $E_m(P_{D1})/E_m(P_{D2})$ difference caused by the six residue pairs. A detailed examination of these residue pairs suggested that, by providing acidic residues of D1 as ligands to the cationic OEC cluster as well as harboring basic residues in the corresponding positions in D2, the entire D1/D2 subunit pair may be energetically stabilized. The larger E_m value for P_{D2} compared to that for P_{D1} might be a consequence of this energetic balance.

Among the residue pairs that contributed to the difference in the $E_m(P_{D1})/E_m(P_{D2})$ values, contributions of the following three residue pairs were notable: D1-Asn181/D2-Arg180, D1-Asn298/D2-Arg294, and D1-Asp61/D2-His61. The D1-Asn181/D2-Arg180 pair not only upshifted $E_m(P_{D1})$ and $E_m(P_{D2})$ significantly (due to D2-Arg180) but also most strongly contributed to the $E_m(P_{D1})/E_m(P_{D2})$ difference which reached a value of 49 mV higher E_m for P_{D2} than P_{D1} (Table 4a). Another D1-Asn/D2-Arg pair, D1-Asn298/D2-Arg294, contributed to the $E_m(P_{D1})/E_m(P_{D2})$ difference by 43 mV (Table 4a), which was comparable with the

Table 4. D1/D2 Residue Pairs Responsible for the $E_m(P_{D1})/E_m(P_{D2})$ Difference[a]

(a) Key Residue Pairs That Increase the $E_m(P_{D1})/E_m(P_{D2})$ Difference (More than 20 mV)[b]

	influences on the E_m values			influences on the E_m values		D1/D2 pair influence		
D1 residues	$E_m(P_{D1})$	$E_m(P_{D2})$	D2 residues	$E_m(P_{D1})$	$E_m(P_{D2})$	$E_m(P_{D1})$	$E_m(P_{D2})$	ΔE_m
D1-Asn181	−8	1	D2-Arg180	69	109	61	110	**49**
D1-Asn298	1	2	D2-Arg294	54	96	55	98	**43**
D1-Asp61	−64	−41	D2-His61	33	50	−31	9	**40**
D1-Glu329	−53	−35	D2-Arg326	49	67	−4	32	**36**
D1-Glu189	−47	−27	D2-Phe188	5	10	−42	−17	**25**
D1-Asp170	−59	−32	D2-Phe169	−4	−9	−63	−41	**22**

(b) Key Residue Pairs That Decrease the $E_m(P_{D1})/E_m(P_{D2})$ Difference (More Than 20 mV)[c]

	influences on the E_m values			influences on the E_m values		D1/D2 pair influence		
D1 residues	$E_m(P_{D1})$	$E_m(P_{D2})$	D2 residues	$E_m(P_{D1})$	$E_m(P_{D2})$	$E_m(P_{D1})$	$E_m(P_{D2})$	ΔE_m
D1-Ala336	2	2	D2-Asp333	−56	−80	−54	−78	**−24**
D1-Met183	13	10	D2-Leu182	18	−1	31	9	**−22**
D1-Asn301	4	2	D2-Asp297	−35	−54	−31	−52	**−21**
D1-Ile320	−2	−1	D2-Lys317	74	52	72	51	**−21**
D1-His332	64	44	D2-Met329	2	2	66	46	**−20**

[a] D1/D2 residue pairs in each line were generated from the protein sequence alignment performed with the CLUSTAL program.[67] ΔE_m represents the $E_m(P_{D1})/E_m(P_{D2})$ difference due to the D1/D2 residue pair, i.e., $E_m(P_{D2}) - E_m(P_{D1})$. [b] These residue pairs are fully conserved in all known D1/D2 sequences. [c] D2-Leu182 is sometimes replaced with Ile, which resulted in no significant changes in the E_m (P_{D1}/P_{D2}) values. Other residue pairs are fully conserved in all known D1/D2 sequences.

contribution of the D1-Asn181/D2-Arg180 pair. The third residue pair that had a large influence on the $E_m(P_{D1})/E_m(P_{D2})$ difference was D1-Asp61/D2-His61, which contributed a difference of 40 mV. All of the above three D1/D2 residue pairs were not OEC ligand residues, and each of them increased the $E_m(P_{D1})/E_m(P_{D2})$ difference by ~40 mV or more by upshifting $E_m(P_{D2})$ with respect to $E_m(P_{D1})$.

Some acidic residues on the D1 side serving as the OEC ligand were also responsible for the difference in the $E_m(P_{D1})/E_m(P_{D2})$ values by ~20 mV because their counterparts on the D2 side were uncharged hydrophobic Phe residue; e.g., see the following pairs D1-Glu189/D2-Phe188 and D1-Asp170/D2-Phe169 (Table 4a).

(b) the $P_{D1}^{\bullet+}/P_{D2}^{\bullet+}$ Ratio. As would be expected, the residues that are responsible for the $E_m(P_{D1})/E_m(P_{D2})$ difference had similar effects on the $P_{D1}^{\bullet+}/P_{D2}^{\bullet+}$ ratio. This was demonstrated by the fact that vanishing the atomic charges of the D1-Asn298/D2-Arg294 pair resulted in a significant decrease in the occupancy of the $P_{D1}^{\bullet+}$ state, resulting in a $P_{D1}^{\bullet+}/P_{D2}^{\bullet+}$ ratio of 61.7/38.3 (Table 3). Similarly, vanishing the D1-Asn181/D2-Arg180 atomic charges also decreased the $P_{D1}^{\bullet+}$ population. The same tendency was observed for the other residue pairs listed in Table 4a (data not shown), and vanishing the atomic charges of all six pairs of "the $E_m(P_{D1})/E_m(P_{D2})$ difference increasing pairs" (listed in Table 4a) resulted in a $P_{D1}^{\bullet+}/P_{D2}^{\bullet+}$ ratio of 28.7/71.3, with $P_{D2}^{\bullet+}$ being the dominant state (note: we fixed the protonation states of all titratable residues when vanishing the atomic charges of the focusing residues). In contrast, vanishing the atomic charges for "the $E_m(P_{D1})/E_m(P_{D2})$ difference decreasing pairs" (listed in Table 4b) resulted in an increase in the $P_{D1}^{\bullet+}$ population (Table 3). Thus, it can be postulated that residue pairs that affect the E_m values of monomeric Chl*a* (i.e., in the absence of electronic coupling between P_{D1}/P_{D2}) have essentially the same influence on the $P_{D1}^{\bullet+}/P_{D2}^{\bullet+}$ ratio of the coupled P_{D1}/P_{D2} pair, as suggested by ENDOR/TRIPLE resonance spectroscopy.[56]

Many of the residue pairs that are responsible for the larger $P_{D1}^{\bullet+}$ population than $P_{D2}^{\bullet+}$ (Table 4a) may also play important roles in tuning $E_m(Y_Z)$ or $E_m(Y_D)$. For the D1-Asn181/D2-Arg180 pair, mutations at the D2-Arg180 residue have been shown to (i) increase the charge recombination rate between Q_A^- and $P680^{\bullet+}$ and (ii) decrease the EPR signal from Y_D.[57]

The importance of D2-Arg294 for stability and function of PSII was suggested from random mutagenesis studies of PSII from *Synechocystis* PCC 6803.[58] PSII with D2-Arg294 mutated to Trp was still capable of O_2 evolution but with an initial rate four times lower than that of wild type and was very sensitive to light, showing a rapid photoinhibition under illumination.[58] Indeed, the D1-Asn298/D2-Arg294 pair is linked to Y_Z/Y_D via the H-bonded partners D1-His190/D2-His189. The positively charged D2-Arg294 prevents protonation of the D2-His189 Nδ atom, whereas D1-Asn298 did not prevent D1-His190 protonation, thus differentiating the protonation state of the His residues, which may contribute to the difference in the $E_m(Y_Z)$ and $E_m(Y_D)$ values significantly.[59]

D1-Asp61 has been proposed to participate in the possible proton exit pathway that guides protons generated from water oxidation to the lumenal bulk solution.[48,60] Its counterpart, D2-His61, has been suggested to alter the protonation state in response to the changes in the $P_{D1}/P_{D2}/Y_D$ redox states.[59] This residue pair may therefore also contribute to the difference in the $E_m(Y_Z)$ and $E_m(Y_D)$ values.

D1-Glu189 was suggested to be involved in a H-bond network with Y_Z and D1-His190;[61,62] mutations of D1-Glu189 yielded PSII complexes that could neither evolve O_2 nor advance the S state beyond the $Y_Z^{\bullet}S_2$ state. This residue was finally confirmed to ligate the Mn1 atom of OEC in the 1.9 Å structure.[25]

dx.doi.org/10.1021/ja203947k |*J. Am. Chem. Soc.* 2011, 133, 14379–14388

Table 5. Ratios of Charge/Spin Distribution in Vacuum (i.e., in the Absence of the Protein Environment) [%][a]

	charge		spin	
	$P_{D1}^{\bullet+}$	$P_{D2}^{\bullet+}$	P_{D1}	P_{D2}
original geometry ($vinyl_{in}/vinyl_{out}$)	57.5	42.5	59.8	40.2
P_{D1}-vinyl replaced by the P_{D2}-vinyl geometry [b] ($vinyl_{out}/vinyl_{out}$)	61.3	38.7	63.3	36.7
P_{D2}-vinyl replaced by the P_{D1}-vinyl geometry [b] ($vinyl_{in}/vinyl_{in}$)	57.9	42.1	61.7	38.3
P_{D1}/P_{D2}-vinyl swapped[b] ($vinyl_{out}/vinyl_{in}$)	61.4	38.6	64.9	35.1
P_{D1}-phytol replaced by the P_{D2}-phytol geometry[b]	51.4	48.6	53.6	46.4
phytol deleted P_{D1}/P_{D2}[b]	53.4	46.6	55.4	44.6

[a] For atomic partial charges of $[P_{D1}/P_{D2}]^{\bullet+}$ (unrestricted DFT/B3LYP functional, LACVP*), see Table S5, Supporting Information. [b] See Figure S1, Supporting Information, for the geometry.

Taken together, these residue pairs are a prerequisite for not only the proper functioning of P680 but also the functioning of Y_Z/Y_D. Indeed, these residue pairs are fully conserved in all known D1/D2 sequences (not shown). Thus, we conclude that the differences in the energetics of P_{D1}/P_{D2} as well as Y_Z/Y_D between the D1 and D2 sides were mainly due to the asymmetry in the electrostatic character of the conserved D1/D2 residue pairs, e.g., D1-Asn181/D2-Arg180,[57] D1-Asn298/D2-Arg294,[58,59] D1-Asp61/D2-His61,[59] and D1-Glu189[61,62]/D2-Phe188.

Compensation of the Mn_4CaO_5 Charge Influence by the Protein Environment. The low $E_m(P_{D1})$ value with respect to the $E_m(P_{D2})$ value appears to be in contrast to the fact that the location of the metal cluster OEC is closer to P_{D1} than P_{D2}: the Mn_4CaO_5 region including Cl^- 1 and 2 is responsible for the $E_m(P_{D1})$ upshift of 174 mV, which is 2-fold greater than the $E_m(P_{D2})$ upshift of 85 mV (Table 1). Nevertheless, the D1 subunit, in turn, downshifts $E_m(P_{D1})$ predominantly (by 238 mV) with respect to $E_m(P_{D2})$ (by 65 mV). In fact, the difference in the upshifts of $E_m(P_{D1})$ and $E_m(P_{D2})$ brought about by the OEC cluster is perfectly compensated for by the downshift due to the OEC acidic ligands that are mainly provided by the D1 subunit, e.g., D1-Glu189/D2-Phe188 and D1-Asp170/D2-Phe169 (Table 4a). Thus, the difference in the OEC charge influence on $E_m(Chla)$ is neither a direct (but maybe an indirect) reason for the $E_m(P_{D1})/E_m(P_{D2})$ difference nor responsible for the asymmetric distribution of the positive charge over the P_{D1}/P_{D2} pair.

Influences of the Orientations of the Vinyl and Phytol Groups on the $P_{D1}^{\bullet+}/P_{D2}^{\bullet+}$ Ratio. If we remove the PSII protein subunits (isolated P_{D1}/P_{D2} pair), the $P_{D1}^{\bullet+}/P_{D2}^{\bullet+}$ ratio (in vacuum) was calculated to be 57.5/42.5 (Table 5). The delocalization of the cationic state among P_{D1} and P_{D2} calculated in vacuum indicates that the electronic coupling is present in PSII. In agreement with the present result, Noguchi and co-workers also observed the delocalization of the cationic state among P_{D1} and P_{D2} in the absence of the PSII protein environment,[55] indicating the presence of the electronic coupling between P_{D1} and P_{D2}. The significantly lowered ratio of $P_{D1}^{\bullet+}/P_{D2}^{\bullet+}$ calculated in vacuum compared with that obtained in PSII proteins suggests that the remarkable asymmetric distribution of the cationic state among P_{D1} and P_{D2} was not due to the geometry of the two chlorophylls but due to the asymmetric protein environment provided by PSII. This is in agreement with the results reported by Okubo et al.[53] based on their FTIR measurements. (Note: The electronic coupling may be weak between P_{D1} and P_{D2} but strong between the geometrically corresponding two BChl*a* in bacterial photosynthetic reaction centers because of mutual overlap of BChl*a* rings I.)

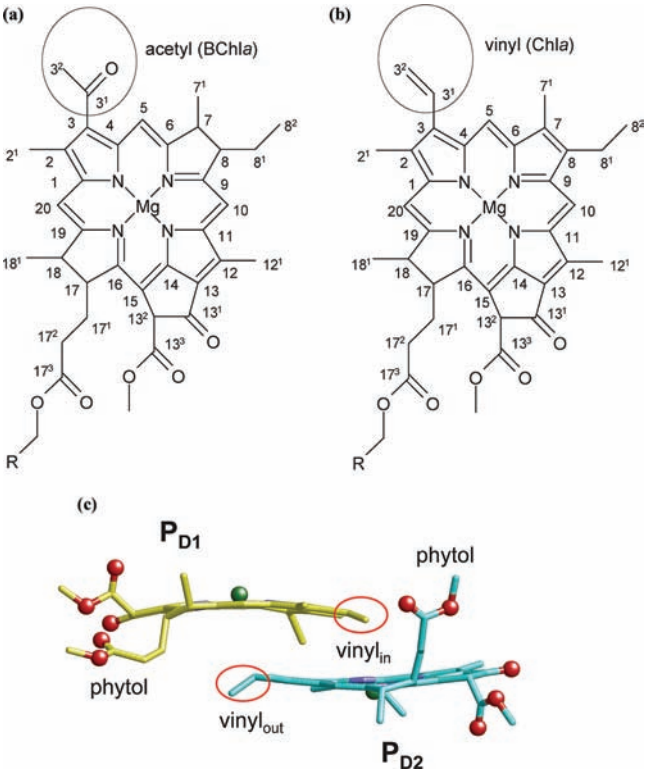

Figure 3. Structure of (a) BChl*a* and (b) Chl*a* with IUPAC numbering scheme (R = phytol chain). (c) Geometry of P_{D1}/P_{D2}. The yellow and the cyan sticks indicate carbon atoms of P_{D1} and P_{D2}, respectively. The red and green spheres represent the oxygen and magnesium atoms, respectively. In quantum mechanical calculations, we replaced the phytol chain region (atoms C1−20) with a methyl group.

In vacuum, the $P_{D1}^{\bullet+}$ population was dramatically decreased relative to that in the PSII proteins but is still the major species (Table 5), implying that the P_{D1}/P_{D2} Chl*a* geometries are not identical in the high-resolution structure of PSII.[25] It was reported that the orientation of the acetyl group of the BChl*a* special pair affects E_m in the bacterial photosynthetic reaction centers.[63] Interestingly, the corresponding group of Chl*a*—the vinyl group—is rather in plane for P_{D1} ($vinyl_{in}$) and out of the plane for P_{D2} ($vinyl_{out}$) in the high-resolution structure of PSII[25] (Figure 3); this subtle difference of the vinyl group orientation between P_{D1} and P_{D2} was revealed for the first time in the present crystal structure at 1.9 Å resolution.[25] In the PSII proteins, adopting the $vinyl_{in}$ conformation for both P_{D1}/P_{D2} leads to a decrease in the $P_{D1}^{\bullet+}$ population,

promoting the electronic coupling and cation delocalization over P_{D1}/P_{D2}, resulting in a P_{D1}/P_{D2} ratio of 70.0/30.0 (see $vinyl_{in}$/$vinyl_{in}$ in Table 3). The influence of the vinyl group orientation of P_{D1} in the $P_{D1}^{\bullet+}/P_{D2}^{\bullet+}$ ratio is somewhat larger than that of P_{D2}, implying a difference in the protein environments or mutual orientation of the Chl*a* molecules.

Another notable difference in the P_{D1}/P_{D2} geometry is at the flipped orientation of the phytol chain with respect to the ester group in the neighborhood (Figure S1, Supporting Information). Modeling the P_{D1} phytol chain orientation as that of P_{D2} leads to a remarkable decrease in the $P_{D1}^{\bullet+}$ population in vacuum (Table 5) as implied from computational studies.[64] Thus, the larger $P_{D1}^{\bullet+}$ population than $P_{D2}^{\bullet+}$ for the isolated P_{D1}/P_{D2} pair in vacuum partially arose from the difference in the phytol chain orientations of the two pigments. However, the P_{D1} phytol chain flip had less contribution (although still notable) to the asymmetric distribution of $P_{D1}^{\bullet+}/P_{D2}^{\bullet+}$ in the PSII proteins (65.5/34.5, Table 3) than in vacuum (51.4/48.6, Table 5). Furthermore, substitution of the P_{D1}/P_{D2} phytol chains with $-CH_3$ group (phytol deleted P_{D1}/P_{D2}) resulted in a $P_{D1}^{\bullet+}/P_{D2}^{\bullet+}$ ratio of 53.4/46.6 in vacuum and of 67.1/32.9 in the PSII protein. Thus, in contrast to vacuum, the phytol chain orientation is not a primary factor in determining the $P_{D1}^{\bullet+}/P_{D2}^{\bullet+}$ ratio in the PSII proteins. The reason that the phytol chain orientation had a larger effect on the $P_{D1}^{\bullet+}/P_{D2}^{\bullet+}$ ratio in vacuum than in proteins is that the interaction of the phytol chain with the ester group is considerably overestimated because the two groups are the only polarized sites for Chl*a* in vacuum.

CONCLUDING REMARKS

Using the high-resolution structure of PSII recently reported, we calculated the E_m values of P_{D1} and P_{D2}, which showed that $E_m(P_{D2})$ is higher than $E_m(P_{D1})$ by ~100 mV. This difference suggests a predominant localization of the cationic state on P_{D1} over P_{D2}. Indeed, we determined the $P_{D1}^{\bullet+}/P_{D2}^{\bullet+}$ ratio to be 76.9/23.1 (80.6/19.4 for spin density distribution) using large-scale QM/MM calculations. This ratio was found to be determined predominantly by the D1/D2 protein environment. This is consistent with the fact that spin density distribution of the chlorophyll pairs can be altered significantly by mutation of the interacting residues.[56,65] It can be concluded therefore that the $P_{D1}^{\bullet+}/P_{D2}^{\bullet+}$ ratio of ~80/~20 is mainly due to the difference in the D1/D2 heterodimer residue pairs that cause the $E_m(P_{D1})/E_m(P_{D2})$ difference. Most of these residue pairs (listed in Table 4a) are fully conserved in all known D1/D2 sequences and are a prerequisite not only for (i) the proper functioning of P680 (D1-Asn181/D2-Arg180[57]) but also for (ii) the functioning of Y_Z/Y_D (D1-Asn181/D2-Arg180,[57] D1-Asn298/D2-Arg294,[58,59] D1-Asp61/D2-His61,[59] and D1-Glu189[25,62]/D2-Phe188), (iii) the possible proton exit pathway that guides protons generated from water oxidation to the lumenal bulk solution (D1-Asp61[48,60]/D2-His61), and (iv) the OEC ligands (D1-Glu189[61,62]/D2-Phe188 and D1-Asp170[66]/D2-Phe169). From the significant contributions of these key residue pairs in terms of the PSII functions, the larger $P_{D1}^{\bullet+}$ population than $P_{D2}^{\bullet+}$ appears to be an inevitable fate of the intact PSII that possesses water oxidation activity.

ASSOCIATED CONTENT

Supporting Information. Atomic charges. This material is available free of charge via the Internet at http://pubs.acs.org.

AUTHOR INFORMATION

Corresponding Author
hiro@cp.kyoto-u.ac.jp

ACKNOWLEDGMENT

This work was supported by the JST PRESTO program (H.I. & M.S.), Grant-in-Aid for Science Research from the Ministry of Education, Science, Sport and Culture of Japan (21770163 to H.I. and 22740276 to K.S.), Special Coordination Fund for Promoting Science and Technology of MEXT (H.I.), Takeda Science Foundation (H.I.), and Kyoto University Step-up Grant-in-Aid for young scientists (H.I.).

REFERENCES

(1) Prokhorenko, V. I.; Holzwarth, A. R. *J. Phys. Chem. B* **2000**, *104* 11563–11578.
(2) Diner, B. A.; Rappaport, F. *Annu. Rev. Plant Biol.* **2002**, *53* 551–580.
(3) Renger, G.; Renger, T. *Photosynth. Res.* **2008**, *98*, 53–80.
(4) Klimov, V. V.; Allakhverdiev, S. I.; Demeter, S.; Krasnovskii, A. A. *Dokl. Akad. Nauk SSSR* **1979**, *249*, 227–230.
(5) Rutherford, A. W.; Mullet, J. E.; Crofts, A. R. *FEBS Lett.* **1981**, *123*, 235–237.
(6) Watanabe, T.; Kobayashi, M. In *Chlorophylls*; Scheer, H., Ed.; CRC Press: Boca Raton, FL, 1991; pp 287−303.
(7) Ohashi, S.; Iemura, T.; Miyashita, H.; Watanabe, T.; Kobayashi, M. *Photomed. Photobiol.* **2008**, *30*, 13–18.
(8) Kobayashi, M.; Ohashi, S.; Fukuyo, S.; Kasahara, M.; Watanabe, T. In *Photosynthesis: Energy from the Sun*; Allen, J. F., Gantt, E., Golbeck, J. H., Osmond, B., Eds.; Springer: New York, 2008; pp 113−116.
(9) Zouni, A.; Witt, H. T.; Kern, J.; Fromme, P.; Krau, N.; Saenger, W.; Orth, P. *Nature* **2001**, *409*, 739–743.
(10) Rappaport, F.; Guergova-Kuras, M.; Nixon, P. J.; Diner, B. A.; Lavergne, J. *Biochemistry* **2002**, *41*, 8518–8527.
(11) Krieger, A.; Rutherford, A. W.; Johnson, G. N. *Biochim. Biophys. Acta* **1995**, *1229*, 193–201.
(12) Johnson, G. N.; Rutherford, A. W.; Krieger, A. *Biochim. Biophys. Acta* **1995**, *1229*, 202–207.
(13) Grabolle, M.; Dau, H. *Biochim. Biophys. Acta* **2005**, *1708* 209–218.
(14) Loll, B.; Kern, J.; Saenger, W.; Zouni, A.; Biesiadka, J. *Nature* **2005**, *438*, 1040–1044.
(15) Ishikita, H.; Saenger, W.; Biesiadka, J.; Loll, B.; Knapp, E.-W. *Proc. Natl. Acad. Sci. U.S.A.* **2006**, *103*, 9855–9860.
(16) Kato, Y.; Sugiura, M.; Oda, A.; Watanabe, T. *Proc. Natl. Acad. Sci. U.S.A.* **2009**, *106*, 17365–17370.
(17) Renger, G.; Holzwarth, A. R. In *Photosystem II*; Wydrqynski, T., Satoh, K., Eds.; Springer: Dordrecht, The Netherlands, 2005; pp 139−175.
(18) Renger, G. In *Primary Processes of Photosynthesis: Principles and Apparatus, Part II*; Renger, G., Ed.; Royal Society Chemistry: Cambridge, UK, 2008; pp 237−290.
(19) Dau, H.; Haumann, M. *Coord. Chem. Rev.* **2008**, *252*, 273–295.
(20) Rappaport, F.; Diner, B. A. *Coord. Chem. Rev.* **2008**, *252* 259–272.
(21) Rigby, S. E. J.; Nugent, J. H. A.; O'Malley, P. J. *Biochemistry* **1994**, *33*, 10043–10050.
(22) Diner, B. A.; Schlodder, E.; Nixon, P. J.; Coleman, W. J.; Rappaport, F.; Lavergne, J.; Vermaas, W. F. J.; Chisholm, D. A. *Biochemistry* **2001**, *40*, 9265–9281.
(23) Michel, H.; Deisenhofer, J. *Biochemistry* **1988**, *27*, 1–7.
(24) Guskov, A.; Kern, J.; Gabdulkhakov, A.; Broser, M.; Zouni, A.; Saenger, W. *Nat. Struct. Mol. Biol.* **2009**, *16*, 334–342.
(25) Umena, Y.; Kawakami, K.; Shen, J.-R.; Kamiya, N. *Nature* **2011**, *473*, 55–60.

(26) Noguchi, T.; Tomo, T.; Inoue, Y. *Biochemistry* **1998**, *37* 13614–13625.
(27) Sugiura, M.; Rappaport, F.; Brettel, K.; Noguchi, T.; Rutherford, A. W.; Boussac, A. *Biochemistry* **2004**, *43*, 13549–13563.
(28) Brooks, B. R.; Bruccoleri, R. E.; Olafson, B. D.; States, D. J.; Swaminathan, S.; Karplus, M. *J. Comput. Chem.* **1983**, *4*, 187–217.
(29) MacKerell, A. D., Jr.; et al. *J. Phys. Chem. B* **1998**, *102* 3586–3616.
(30) Rabenstein, B.; Ullmann, G. M.; Knapp, E.-W. *Eur. Bophys. J.* **1998**, *27*, 626–637.
(31) Bayly, C. I.; Cieplak, P.; Cornell, W. D.; Kollman, P. A. *J. Phys. Chem.* **1993**, *97*, 10269–10280.
(32) *Jaguar*, version 7.5; Schrödinger, LLC: New York, NY, 2008.
(33) Bashford, D.; Karplus, M. *Biochemistry* **1990**, *29*, 10219–10225.
(34) Ishikita, H.; Biesiadka, J.; Loll, B.; Saenger, W.; Knapp, E. W. *Angew. Chem., Int. Ed. Engl.* **2006**, *45*, 1964–1965.
(35) Rabenstein, B.; Knapp, E. W. *Biophys. J.* **2001**, *80*, 1141–1150.
(36) Kobayashi, M.; Ohashi, S.; Iwamoto, K.; Shiraiwa, Y.; Kato, Y.; Watanabe, T. *Biochim. Biophys. Acta* **2007**, *1767*, 596–602.
(37) Fajer, J.; Fujita, I.; Davis, M. S.; Forman, A.; Hanson, L. K.; Smith, K. M. In *Electrochemical and spectrochemical studies of biological redox components*; Kadish, K. M., Ed.; American Chemical Society: Washington, D.C., 1982; Chapter 21.
(38) Maggiora, L. L.; Petke, J. D.; Gopal, D.; Iwamoto, R. T.; Maggiora, G. M. *Photochem. Photobiol.* **1985**, *42*, 69–75.
(39) Cotton, T. M.; van Duyne, R. P. *J. Am. Chem. Soc.* **1979**, *101* 7605–7612.
(40) Wasielewski, M. R.; Smith, R. L.; Kostka, A. G. *J. Am. Chem. Soc.* **1980**, *102*, 6923–6928.
(41) *QSite*, version 5.6; Schrödinger, LLC: New York, NY, 2010.
(42) Ludwig, M. L.; Pattridge, K. A.; Metzger, A. L.; Dixon, M. M.; Eren, M.; Feng, Y.; Swenson, R. P. *Biochemistry* **1997**, *36*, 1259–1280.
(43) Ishikita, H. *J. Biol. Chem.* **2007**, *282*, 25240–25246.
(44) Yeates, T. O.; Komiya, H.; Chirino, A.; Rees, D. C.; Allen, J. P.; Feher, G. *Proc. Natl. Acad. Sci. U.S.A.* **1988**, *85*, 7993–7997.
(45) Ermler, U.; Fritzsch, G.; Buchanan, S. K.; Michel, H. *Structure* **1994**, *2*, 925–936.
(46) Stowell, M. H. B.; McPhillips, T. M.; Rees, D. C.; Solitis, S. M.; Abresch, E.; Feher, G. *Science* **1997**, *276*, 812–816.
(47) Breton, J.; Boullais, C.; Burie, J. R.; Nabedryk, E.; Mioskowski, C. *Biochemistry* **1994**, *33*, 14378–14386.
(48) Iwata, S.; Barber, J. *Curr. Opin. Struct. Biol.* **2004**, *14*, 447–453.
(49) Ferreira, K. N.; Iverson, T. M.; Maghlaoui, K.; Barber, J.; Iwata, S. *Science* **2004**, *303*, 1831–1838.
(50) Ishikita, H.; Knapp, E.-W. *J. Biol. Chem.* **2005**, *280*, 12446–12450.
(51) Service, R. J.; Hillier, W.; Debus, R. J. *Biochemistry* **2010**, *49* 6655–6669.
(52) Vassiliev, S.; Comte, P.; Mahboob, A.; Bruce, D. *Biochemistry* **2010**, *49*, 1873–1881.
(53) Okubo, T.; Tomo, T.; Sugiura, M.; Noguchi, T. *Biochemistry* **2007**, *46*, 4390–4397.
(54) Plato, M.; Krauss, N.; Fromme, P.; Lubitz, W. *Chem. Phys.* **2003**, *294*, 483–499.
(55) Takahashi, R.; Hasegawa, K.; Noguchi, T. *Biochemistry* **2008**, *47*, 6289–6291.
(56) Müh, F.; Lendzian, F.; Roy, M.; Williams, J. C.; Allen, J. P.; Lubitz, W. *J. Phys. Chem. B* **2002**, *106*, 3226–3236.
(57) Manna, P.; LoBrutto, R.; Eijckelhoff, C.; Dekker, J. P.; Vermaas, W. *Eur. J. Biochem.* **1998**, *251*, 142–154.
(58) Ermakova-Gerdes, S.; Yu, Z.; Vermaas, W. *J. Bacteriol.* **2001**, *183*, 145–154.
(59) Ishikita, H.; Knapp, E. W. *Biophys. J.* **2006**, *90*, 3886–3896.
(60) Ishikita, H.; Saenger, W.; Loll, B.; Biesiadka, J.; Knapp, E.-W. *Biochemistry* **2006**, *45*, 2063–2071.
(61) Chu, H.; Nguyen, A. P.; Debus, R. J. *Biochemistry* **1995**, *34*, 5839–5858.
(62) Debus, R. J.; Campbell, K. A.; Pham, D. P.; Hays, A. M.; Britt, R. D. *Biochemistry* **2000**, *39*, 6275–6287.
(63) Muegge, I.; Apostolakis, J.; Ermler, U.; Fritzsch, G.; Lubitz, W.; Knapp, E.-W. *Biochemistry* **1996**, *35*, 8359–8370.
(64) Yamasaki, H.; Takano, Y.; Nakamura, H. *J. Phys. Chem. B* **2008**, *112*, 13923–13933.
(65) Witt, H.; Schlodder, E.; Teutloff, C.; Niklas, J.; Bordignon, E.; Carbonera, D.; Kohler, S.; Labahn, A.; Lubitz, W. *Biochemistry* **2002**, *41*, 8557–8569.
(66) Nixon, P. J.; Diner, B. A. *Biochemistry* **1992**, *31*, 942–948.
(67) Higgins, D. G.; Thompson, J. D.; Gibson, T. J. *Methods Enzymol.* **1996**, *266*, 383–402.